Onset of electroconvection in nematic liquid crystals with parallel magnetic field

J. T. Gleeson
Department of Physics and Astronomy, The University of Calgary, Calgary, Alberta, Canada T2N 1N4
(Received 16 April 1996; revised manuscript received 16 July 1996)

We report experiments measuring the threshold electric field for electrohydrodynamic instabilities in nematic liquid crystals as a function of magnetic field applied parallel to the electric field. At low magnetic fields, the threshold voltage decreases in quantitative agreement with theoretical predictions. However, at higher magnetic fields, a crossover is seen and the threshold voltage increases linearly with the magnetic field. In this region, the bifurcation from conduction to convection is subcritical, with the discontinuity increasing linearly with magnetic field. The wavelength exhibited by the roll structure at onset also increases dramatically with the applied magnetic field. [S1063-651X(96)02812-7]

PACS number(s): 61.30.Eb, 47.20.Ky, 47.54.+r

I. INTRODUCTION

Pattern formation in nonlinear, nonequilibrium dynamical systems is a subject of intense, recent activity [1]. Of particular interest are systems which exhibit structures periodic in one dimension only; electrohydrodynamic convection (EHC) in nematic liquid crystals [2,3] is one such system. This system has distinct advantages over more traditional pattern forming systems like Rayleigh-Bénard [1] convection or Taylor vortex flow [4], because it typically contains thousands of periods in the structure, reducing the effect of lateral boundaries. In addition, the time scales for the pattern to reach steady state can be orders of magnitude smaller than in other convection systems. One important difference is that because of the intrinsic anisotropy of the liquid crystal, the roll structure in EHC has a preferred direction, which is not the case in thermal convection. Much work to date has focused on the structure and dynamics exhibited by this system in response to changes in both the frequency and the amplitude of the electric field driving the system unstable [3]. Most reported experiments in which a magnetic field is used in addition to the electric field have concentrated on the case where the magnetic field is perpendicular to the electric field [5,6]. We report on experiments in which the magnetic field is parallel to the electric field [7,8]. In the undistorted configuration the nematic director is parallel to $\hat{\mathbf{x}}$, while the applied electric and magnetic fields are both parallel to $\hat{\mathbf{z}}$. The original motivation for beginning these experiments was to seek analogies with thermal convection in binary fluids having negative separation ratio in which the Soret effect acts as a stabilizing influence against the destabilizing temperature gradient. We demonstrate some effects in common with those seen in binary fluid convection [9], however we shall see that it would be exceedingly premature to try to exploit further any analogies.

II. EXPERIMENTS

The experimental arrangement is in many ways the ''classical setup'' [3,10]. A liquid crystalline compound with negative dielectric anisotropy and positive conductivity anisotropy is introduced between transparent conducting electrode plates in a parallel plate capacitor geometry. The electrodes are treated so that the nematic director is everywhere in the $\hat{\mathbf{x}}$ direction when there are no external fields. Homogeneous (planar) alignment of sample cells was obtained by evaporating 200 Å of SiO at an angle of 60° to the substrate normal [11]. The substrates were indium-tin-oxide (ITO) coated, float-glass plates. After evaporation, the plates were clamped together with Mylar spacers between them, and then bonded together with Torr-Seal epoxy. The plate separation was 50 μm, and the conducting area of the plates was roughly 2 cm$\times$2 cm. Methoxy-benzylidene butylaniline (MBBA) [12] (used without further purification) was introduced between the plates via capillary action, and the uniformity of the alignment checked by microscopy between crossed polarizers. The finished sample is inserted into a copper block having a hole drilled for optical access. The temperature of the block is controlled within $\pm$0.01 °C with circulating water. In all experiments reported here, the temperature of the sample was 30.00 °C. The clearing point of the liquid crystal was 37 °C, and the cutoff frequency was 730 Hz.

The thermostatted sample holder is placed in the gap of an electromagnet having a 2.5 cm hole drilled through its pole faces for optical access. The gap between faces is 22.5 cm and their diameter is 30.0 cm. With this configuration, the magnetic field is constant within 0.5% over the space occupied by the liquid crystal sample. This was verified by mounting a small Hall probe on a three-axis translator and measuring the change in the magnetic field as the probe was moved a distance comparable to the sample size. The field is servo controlled and is stable to within 0.05 G. A sinusoidal electric field is applied with a function generator via the ITO coatings; a capacitor in series is used to eliminate dc offset. For all experiments reported here, a frequency of 100 Hz was used. The convective roll structure is imaged via the shadowgraph technique using a Questar QM-1 long distance microscope equipped with a charge coupled devices (CCD) video camera. To enhance contrast, the incident light was linearly polarized at 45° to $\hat{\mathbf{x}}$. The experimental configuration is depicted schematically in Fig. 1. The video signal is digitized with a frame-grabber for further analysis, described subsequently. The clearing point and the threshold field for the Fréedericksz transition are determined by replacing the microscope with a photodetector and monitoring the inten-

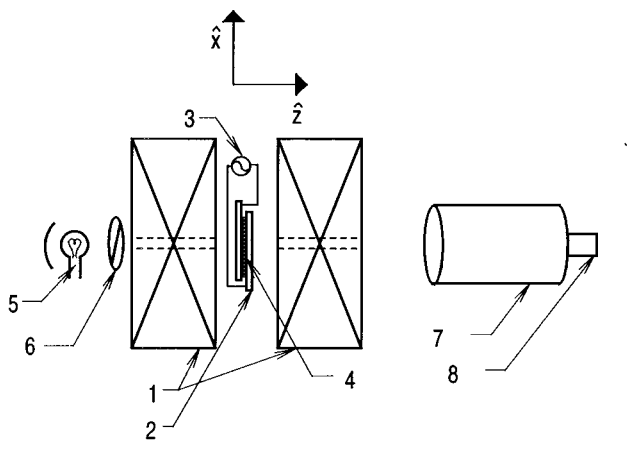

FIG. 1. Schematic of experimental setup. Legend: (1) electromagnet, (2) conducting glass substrates, (3) function generator, (4) liquid crystal, (5) light source, (6) polarizer, (7) long distance microscope, and (8) CCD video camera.

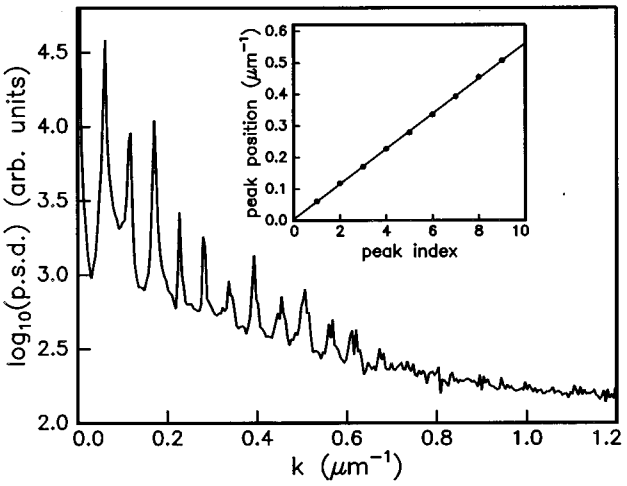

FIG. 2. Example of power spectral density data. The inset shows the peak positions as function of index. The slope of the best fit straight line gives the wavelength to better than single pixel accuracy

sity of light transmitted through the sample when it is placed between crossed polarizers.

The experimental protocol for examining the behavior of the system near onset is to select the magnetic field, then very slowly ramp the electric field up, then down. At each step in the electric field, after a prescribed waiting period, the video signal is digitized. Since we are primarily interested in patterns that have a periodicity perpendicular to the alignment direction $\hat{\mathbf{x}}$ our analysis technique focuses on those features. This analysis is particularly suitable because the first instability observed in this system is to normal rolls. Each video line in this direction is analyzed with the fast Fourier transform, and the results are added bin by bin to give an average power spectral density (PSD) for structures periodic in one direction only. This analysis ignores any structures not perpendicular to the alignment direction, and so is not useful for detecting secondary instabilities. In fact, when such instabilities occur, they can lead to a loss of signal for this technique. Hence it is well suited only for characterizing the onset of convection. The transmission of light through a thin layer of nematic liquid crystal undergoing a periodic deformation of the director in the direction perpendicular to the incident light [$\theta(x) \propto \theta_0 \cos(kx)$] is considered in detail in Ref. [13]. The intensity of transmitted light $I(x)$ can be expressed as

$$I(x) = \frac{I_0}{1 + c_1 \theta_0 \cos(kx) + c_2 \theta_0^2 \sin(2kx)}, \tag{1}$$

where $2\pi/k$ is the periodicity of the director distortion, and the c's are constants determined chiefly by the indices of refraction and the geometry of the imaging system. Since this function is periodic in x, it can be expressed as a Fourier series

$$I(x) = \sum_{m=0} a_m \exp(imkx). \tag{2}$$

The coefficients a_m for nonzero m can all be written in the form $\theta_0 P_m(\theta_0)$, where $P_m(\theta_0)$ is a polynomial. These polynomials can be determined by straightforward, although tedious, calculation. The power spectral density of the intensity of transmitted light should then be a series of peaks, each occuring at an integer multiple of the fundamental k, with the height of the mth peak being proportional to $|a_m|^2$. Equally straightforward, but even more tedious, would be to use the heights of all visible peaks to solve the coefficients a_m for θ_0; this is not necessary for the present aims of these experiments. We take the sum of the heights of the visible peaks in the PSD as the unambiguous signal of the onset of convection; let us call this quantity $S(\theta_0)$. Any quantity that is a continuous function of $S(\theta_0)$ will also be a continuous function of θ_0. Note however that any quantity monotonically increasing with θ_0 may not monotonically increase with $S(\theta_0)$. An added benefit of this method is that detecting the onset of convection can be fully automated.

The periodicity of the pattern can also be accurately obtained from the power spectrum. If we plot the position of all peaks observed in the power spectrum as a function of their index, the slope of the resulting line allows us to determine k with an accuracy smaller than the width of a single pixel. Figure 2 shows an example of power spectral density (PSD); the inset shows the peak positions as a function of peak index, and the solid line is the best fitting straight line.

III. RESULTS

As the magnetic field H is varied, the onset of EHC is strongly affected, but in qualitatively different ways, depending on the magnitude of the applied magnetic field. For magnetic fields lower than a special level H_C, of which more is said subsequently, the transition from the quiescent state to convection is qualitatively the same as the zero magnetic field case. In Fig. 3 we plot our measure of the amplitude of periodic director distortion, $S(\theta_0)$ vs applied voltage V, for both increasing and decreasing voltage, at $H = 0.271$ kG.

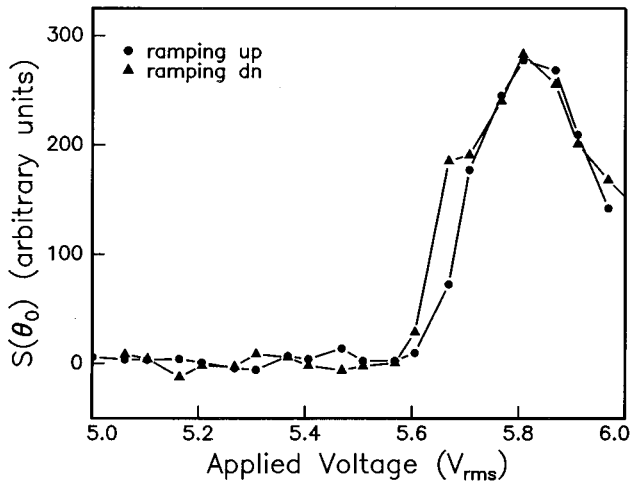

FIG. 3. $S(\theta_0)$ as a function of applied voltage at $H=0.271$ kG. Note that $S(\theta_0)$ is not strictly zero below the convection threshold. This is because the automated method of finding peaks also finds noise peaks that are present. Since the actual peaks are so much larger (cf. Fig. 2) we see a large increase at the onset of convection.

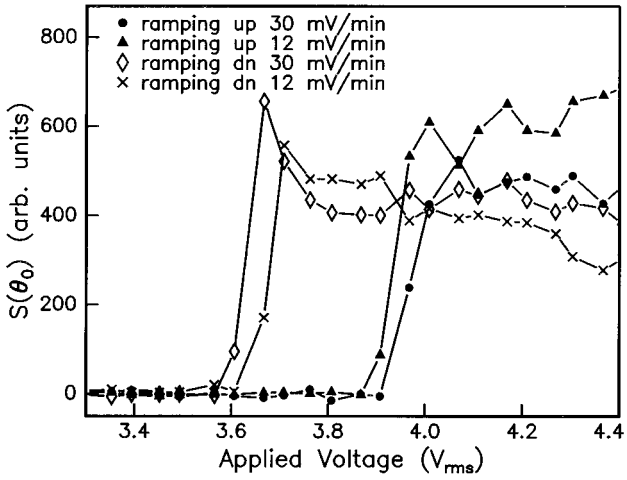

FIG. 4. $S(\theta_0)$ as a function of applied voltage at $H=1.755$ kG at different ramp rates. Here there is a marked dependence on ramping rate, and a very large hysteresis.

$S(\theta_0)$ increases continuously from zero when V exceeds at a critical value V_c. This behavior is consistent with the results presented in Ref. [13] in which θ_0 was found to increase with V^2/V_c^2-1 in the manner expected for a supercritical, pitchfork bifurcation. Note that the same V_c is observed for both increasing and decreasing V. V_c does depend strongly on H; that dependence is discussed subsequently. Note that above the onset voltage, $S(\theta_0)$ is no longer strictly monotonically increasing. This is observed for several reasons: any secondary instabilities above the bifurcation to normal rolls lead to a diminution of $S(\theta_0)$, also, as the convection amplitude becomes larger, in some regions the shadowgraph focusing or defocusing is strong enough to cause the CCD and/or the analog-to-digital converter in the frame grabber to, respectively, saturate or appear completely dark, because of insufficient dynamic range. This is why this technique is useful mainly to detect the onset of convection. The onset of convection predicted by this technique is invariably confirmed visually.

For $H>H_C$ the onset of EHC is dramatically different from that discussed above, and becomes more so as $H-H_C$ increases. Figure 4 shows $S(\theta_0)$ vs V at $H=1.755$ kG; different rates of ramping the voltage both up and down are shown. There are several features to point out here. Concentrating just on the ramping-up data reveals a different apparent threshold voltage to achieve convection for different ramp rates. The largest apparent threshold voltage is measured for the lowest ramp rate. This is because of the dynamics of how convection arises, which are discussed later. A far larger effect, however, is the difference between the voltage at which convection appears when V is increasing, which we shall refer to as $V_A(H)$, and the voltage at which convection disappears when V is decreasing $[V_D(H)]$. Furthermore, in the ramping-up data, we observe a very abrupt increase in $S(\theta_0)$ as V exceeds $V_A(H)$, and, upon ramping down, a correspondingly abrupt decrease in $S(\theta_0)$ as V approaches $V_D(H)$. These observations alone strongly indicate that for $H>H_C$, the bifurcation from the quiescent state to EHC is subcritical. Note that this is qualitatively different from the subcritical transition to EHC reported in Ref. [14]. Note also other researchers have studied the transition to convection from the bend Fréedericksz distorted state [15,16], but have reported no evidence of a strongly subcritical bifurcation.

The growth mechanism whereby EHC arises in this high magnetic field regime unambiguously demonstrates that the bifurcation is subcritical. This is seen most clearly if the applied voltage is abruptly raised from zero to some value slightly above V_A. Figure 5 shows space-time plots [17] which demonstrate the different growth mechanisms below and above H_c. Below H_c, the convective rolls grow everywhere simultaneously; the contrast indicating periodic director distortion grows continuously from zero. Above H_c, the rolls appear via the front propagation mechanism. Furthermore, they grow via the transit of rolls having a well-defined tip within which the contrast changes abruptly. Front propagation as a growth mechanism is well known [18] and invariably indicates either a first-order phase transition [19] in equilibrium systems or a subcritical bifurcation [20] in nonequilibrium systems.

Clearly, between the two regimes described above, there must be a tricritical point, where supercritical behavior crosses over to subcritical. This tricritical point occurs at $H_C=1.585$ kG. Moreover, the apparent discontinuity between the conduction state and the convection state increases as H is increased above H_C. Figure 6 shows the combined results of experiments like those whose results are depicted in Figs. 3 and 4. We have plotted both V_A and V_D. For V_A the value plotted is that obtained using the *lowest* ramp rate while for V_D the plotted value corresponds to the *highest* ramp rate; the reasons for this are discussed below. V_A-V_D increases roughly linearly with $H-H_C$. Below H_C, these two values of the applied voltage are the same. We shall refer to the curve corresponding to $V_A(H)$ as the EHC transition line.

Also shown on this plot is the voltage at which the splay

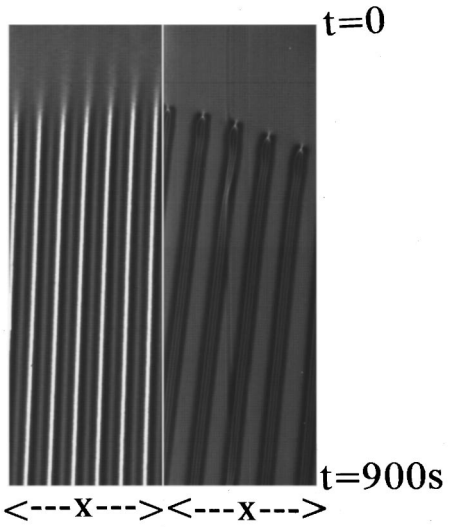

FIG. 5. Space-time plot comparing the growth mechanisms for convective rolls above and below H_C. Both plots correspond to a total elapsed time of 900 seconds. The left was obtained with no magnetic field, and the right at $H=1.960$ kG. At low magnetic fields, the contrast from the periodic director structure grows continuously from zero and homogeneously. At high magnetic fields, the pattern arises via the sequential elongation of individual rolls each of which has an abrupt tip. In both cases, the applied voltage was abruptly raised from zero to a value slightly above V_A, at time $t=0$, as labeled.

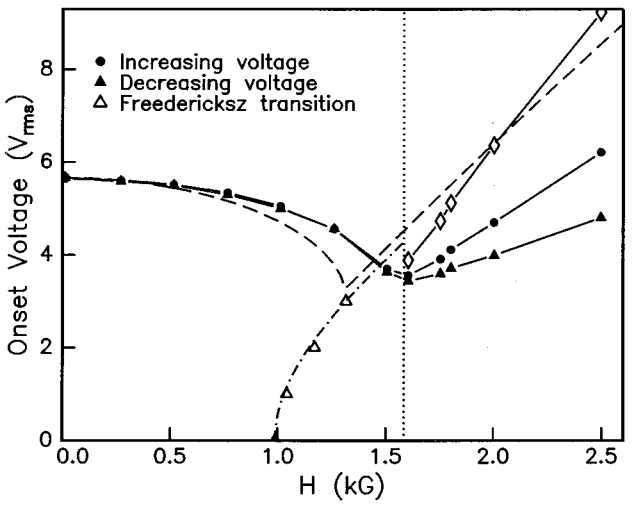

FIG. 6. Voltage at which the convective roll structures either appears or disappears as a function of applied magnetic field. This is determined by monitoring the appearance of peaks in the PSD. The dashed line is from the linear stability calculation of [22]. The minimum in these curves occurs at $H=1.585$ kG, which we call H_c (dotted line on graph). Slightly below H_c, there is a tricritical field, above which the roll pattern appears and disappears at different voltages. The difference between these voltages increases roughly linearly with the magnetic field. The open triangles are the applied voltage at which the splay Fréedericksz transition is observed as a function of magnetic field. The dot-dash line is the extrapolation of this curve to the region above the onset curves. The diamonds are the calculated V_C as described in the text.

Fréedericksz transition occurs, $V_F(H)$. We have included the extrapolation of this curve above the EHC transition line even though EHC occurs before the Fréedericksz transition in this regime. While more sophisticated methods [22] can be used to extrapolate this line, we find the simplest form ($\Delta\chi H^2+\Delta\epsilon V_F^2/d^2=\text{const}$), fits the data satisfactorily. As expected, the critical magnetic field for this transition increases with the applied electric field because the negative dielectric anisotropy stabilizes the planar state. Perhaps the most significant observation to be made from Fig. 6 is that the Fréedericksz transition line crosses the EHC transition line at a value of H within 7% of H_C.

Figure 7 shows the wavelength of the observed pattern as near to onset as practical [21] as a function of the applied magnetic field. Overlaid on this fit are the expected values from the linear stability theory [22]. For fields above H_C, the wavelength increases to about *twice* its value in zero field. The calculated wavelength shows systematic quantitative discrepancies with the measured values, but, qualitatively, the shape of the two curves is reasonably similar. At low magnetic fields, both exhibit a roughly parabolic increase with H, although the theoretical curve's slope almost diverges at H_C. At high fields, both curves show the wavelength not increasing much with H, but the theoretical curve has a dip that is not seen in the data. Furthermore, the calculated value of H_C is significantly smaller than that observed; the reason for this is not yet understood.

IV. DISCUSSION

Also overlaid on Fig. 6 are the results of a linear stability calculation [22] similar to that of Bodenschatz, Zimmermann, and Kramer [24]. In this calculation, the value of the conductivity anisotropy, $\Delta\sigma/\sigma_\perp$ was adjusted to 0.708 [23], to give the observed onset voltage in a zero magnetic field, and the charge relaxation time adjusted to give the correct

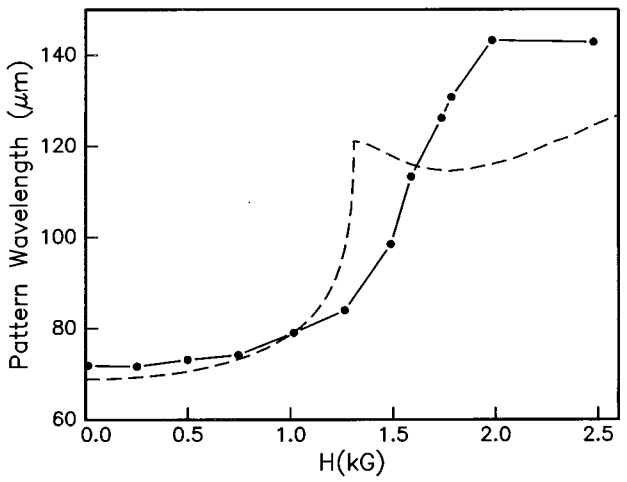

FIG. 7. Wavelength of the roll pattern just above onset as a function of applied magnetic field. Wavelength is determined by the peak positions in the PSD of the image. Note that above 2.5 kG, the roll pattern is often not well organized, so the wavelength is more difficult to determine unambiguously. The dashed line is from the linear stability analysis of [22].

cutoff frequency. For all other parameters the standard values of material constants for MBBA were used [24].

The observation that the Fréedericksz transition line and the EHC transition line cross each other so close to the tricritical point, is in our opinion, unambiguous demonstration that the tricritical point occurs because of the different ''ground states'' from which convection arises. This claim is strongly supported by the observation that the Fréedericksz line crosses the EHC transition line so close to $H=H_C$. On the right-hand side (RHS) of the Fréedericksz line, the nonconvecting, quiescent state is the homogeneous, planar aligned state, while on the left-hand side, (LHS) it is the Freedericksz distorted state in which the director angle with $\hat{z}$ depends on the distance from the glass substrates.

For low magnetic fields, the qualitative agreement with theory for both V_A and k, with only one freely adjusted parameter, indicates that our understanding of the effect of a weak parallel magnetic field on the normal roll instability in EHC of nematics is on reasonably firm ground. However, the situation is much less clear for magnetic fields larger than that where the splay Fréedericksz transition should occur; substantial quantitative discrepancies remain between the calculated critical voltage and V_A.

One possible explanation for this discrepancy may lie in the dynamics of how the convective state invades the quiescent state. The crux of this argument is to recognize that V_C, that voltage where the $\theta_0=0$ state becomes linearly unstable, can be significantly greater than either V_A or V_D, although V_C is what has been calculated. We model the growth of the convection state using the simplest Landau equation that will yield a subcritical bifurcation

$$\frac{\partial\theta_0}{\partial t}=\epsilon\theta_0+g\theta_0^3-g'\theta_0^5, \tag{3}$$

where $\epsilon=(V^2-V_C^2)/V_C^2$ and both g and g' are positive. Note that in principle, g, g', and V_c can all depend on H. Since the value of V_A measured depends on the ramping rate, we take the value obtained at the *lowest* ramping rate and argue that this corresponds to the neutrally stable value of ϵ, ϵ_0. By neutrally stable we mean that the quantity F changes sign at $\epsilon=\epsilon_0$, where $-\delta F/\delta\theta_0$ is the RHS of Eq. (3). A straightforward calculation gives $\epsilon_0=-3g^2/16g'$. This implies that the convection state nucleates and grows at negative ϵ and, hence, a lower voltage than V_C, the voltage where the quiescent state would be linearly unstable. The nucleation of the convection state is very likely caused by, and, hence, located at, microscopic imperfections in the alignment layer on the glass substrates. Furthermore, we identify V_D, the voltage at which convection disappears, with the value of ϵ at which the convection state becomes linearly unstable, sometimes called the saddle node ϵ_u. No convection can exist for $\epsilon<\epsilon_u$. Another simple calculation gives $\epsilon_u=-g^2/4g'$. Since we know neither g nor g', we set $(V_A^2-V_C^2)/V_C^2=\epsilon_0$ and $(V_D^2-V_C^2)/V_C^2=\epsilon_u$ and solve for V_C, obtaining $V_C=\sqrt{4V_A^2-3V_D^2}$. This value for V_C is denoted by the diamond symbols on Fig. 6. The agreement with theory is substantially improved; while V_A is clearly not well described by the theoretical result for V_C, the value of V_C obtained in the manner described is far closer to the theoretical result.

In conclusion, we have demonstrated that a magnetic field parallel to the electric field in EHC can both destabilize or stabilize the quiescent state against convection, depending on its magnitude. Low magnetic fields destabilize in reasonable agreement with linear stability theory. Linear stability theory also satisfactorily predicts the roll spacing for low magnetic fields. High magnetic fields stabilize, and also cause the initial instability to be subcritical.

ACKNOWLEDGMENTS

We have benefited from discussions with A. Hertrich, L. Kramer, A.L. Nip, W. Pesch, and J. Tuszynski. Technical assistance was provided by A. Read, L. Murdock, and D. Todorović-Marinić. This work was supported by the Natural Sciences and Engineering Research Council and the University of Calgary.

[1] M.C. Cross and P.C. Hohenberg, Rev. Mod. Phys. **65**, 851 (1993).

[2] L. Kramer and W. Pesch, *Pattern Formation in Liquid Crystals*, edited by A. Buka and L. Kramer (Springer, New York, 1995).

[3] See, I. Rehberg, B.L. Winkler, M. de la Torre-Juarez, S. Rasenat, and W. Schöpf, Festkörperprobleme **29**, 35 (1989) and references therein.

[4] D.S. Cannell, M.A. Dominguez-Lerma, and G. Ahlers, Phys. Rev. Lett. **50**, 1365 (1983).

[5] S. Kai, N. Chizumi, and M. Kohno, Phys. Rev. A **40**, 6554 (1989).

[6] J.P. McClymer, Molec. Cryst. Liq. Cryst. **199**, 233 (1991).

[7] S. Kai and W. Zimmermann, Prog. Theor. Phys. Suppl. **99**, 458 (1989).

[8] J.T. Gleeson and M. Todorović-Marinić, Molec. Cryst. Liq. Cryst. **256**, 327 (1995).

[9] See, R. Heinrichs, G. Ahlers, and D.S. Cannell, Phys. Rev. Lett. **35**, 2761 (1987); P. Kolodner, C.M. Surko, and H. Williams, Physica D **37**, 319 (1989) for descriptions of the subcritical bifurcation from the quiescent state.

[10] A. Joets and R. Ribotta, Phys. Rev. Lett. **60**, 2164 (1988).

[11] J.L. Janning, Appl. Phys. Lett. **40**, 173 (1972).

[12] Frinton Laboratories, Vineland, N.J.

[13] S. Rasenat, G. Hartung, B.L. Winkler, and I. Rehberg, Exp. Fluids **7**, 412 (1989).

[14] I. Rehberg, S. Rasenat, M. de la Torre Juárez, W. Schöpf, F. Hörner, G. Ahlers, and H.R. Brand, Phys. Rev. Lett. **67**, 596 (1991).

[15] H. Richter, N. Klöpper, A. Hertrich, and A. Buka, Europhys. Lett. **30**, 37 (1995).

[16] A. Hertrich, W. Decker, W. Pesch, and L. Kramer, J. Phys. (France) II **2**, 1915 (1992).

[17] A single video line parallel to $\hat{x}$ is digitized at periodic inter-

vals. The space-time plot is reconstructed by plotting all video lines in sequence as one descends the page. This shows the evolution of the roll structure in one spatial direction very compactly.

[18] W. van Saarloos, Phys. Rev. A **39**, 6367 (1989).

[19] P.E. Cladis, W. van Saarloos, D. Huse, J.S. Patel, J.W. Goodby, and P.L. Finn, Phys. Rev. Lett. **62**, 1764 (1989).

[20] M.F. Schatz, S.J. VanHook, W.D. McCormick, J.B. Swift, and H.L. Swinney, Phys. Rev. Lett. **75**, 1938 (1995).

[21] One must be slightly above onset so that there is sufficient contrast to accurately determine the wavelength.

[22] A. Hertrich, W. Pesch, and J.T. Gleeson, Europhys. Lett. **34**, 417 (1996).

[23] The conductivities were not measured for these experiments, but the value of $\Delta\sigma/\sigma_{\perp}$ quoted is not outside the range of reported measurements. See, I.W. Smith, Y. Galerne, S.T. Lagerwall, E. Dubois-Violette, and G. Durand, J. Phys. **36**, C1-236 (1975).

[24] E. Bodenschatz, W. Zimmermann, and L. Kramer, J. Phys. **49**, 1875 (1988).